CERN-PBC-NOTE-2022-004

2022-03-29

a.ge@cern.ch

RF-Separated Beam Project for the M2 Beam Line at CERN

A. Gerbershagen [1,2], V. Andrieux[3], J. Bernhard[1], M. Brugger[1], O. Denisov[4], J. Friedrich[5], L. Gatignon[6], F. Gerigk[1], A. Guskov[7], B. Ketzer[8], F. Metzger[1,8], W.-D. Nowak[9], C. Quintans[10], S. Schuh[1]

[1] European Organisation for Nuclear Research (CERN), Meyrin, Switzerland

[2] PARTREC, UMCG, University of Groningen, The Netherlands

[3] University of Illinois at Urbana-Champaign, Dept. of Physics, Urbana, USA

[4] National Institute for Nuclear Physics (INFN), Turin, Italy

[5] Technical University of Munich, Department of Physics, 85748 Garching, Germany

[6] Lancaster University, Physics Department, UK

[7] Joint Institute for Nuclear Research, Dubna, Russian Federation

[8] Universität Bonn, Helmholtz-Institut für Strahlen- und Kernphysik, 53115 Bonn, Germany

[9] Universität Mainz, Institut für Kernphysik, 55099

[10] LIP, 1649-003 Lisbon, Portugal

Keywords: Fixed Target Experiment, Kaon Physics, Beamline, RF

Abstract

Within the framework of the Physics Beyond Colliders initiative at CERN, discussions are underway on the feasibility of producing radio-frequency (RF) separated beams for Phase-2 of the AMBER experiment at the M2 beam line in the North experimental area of the CERN SPS. The technique of RF separation is applied to enrich the content of a certain particle type within a beam consisting of different species at the same momentum. It relies on the fact that each particle type has a different velocity, decreasing with rest mass. The successor of the COMPASS experiment, AMBER, requires for its Phase-

2 measurements high-intensity, high-purity kaon (and antiproton) beams, which cannot be delivered with the currently existing conventional M2 beam line. The present contribution introduces the principle of RF separation and explains its dependence on different parameters of beam optics and hardware. The first examination of potential showstoppers for the RF-separated beam implementation is presented, based on the particle production rates, beam line transmission for specific optics settings, limitations for overall beam intensity and purity posed by beam line acceptance and radiation protection. Different beam optics settings have been examined, providing either focused or parallel beams inside the RF cavities. The separation and transmission capability of the different optics settings for realistic characteristics of RF cavities are discussed and the preliminary results of the potential purity and intensity of the RF-separated beam are presented. They illustrate the high importance of an RF-separated kaon beam for many of the AMBER Phase-2 data taking programs, such as spectroscopy, prompt-photon production, Primakoff reactions and kaon charge-radius measurement.

Contents

1 Introduction: CERN North Area 1
1.1 CERN Accelerator Complex 1
1.2 SPS Extraction into the North Area 1
1.3 Kaon and Antiproton Rates in the M2 Beam Line 3
2 Beam Requirements for Phase-2 of the AMBER Experiment 5
3 RF Separated Beam for M2 8
3.1 RF frequency and phase 9
4 M2 Beam Line Considerations 11
4.1 Different Beam Optics Settings Scenarios 11
4.2 Proposed Beam Line Optics 13
4.3 Conclusions from Beam Line Optics Examination 19
5 RF Cavities & RF Power 19
5.1 Cavity requirements 19
5.2 RF power 20
5.3 RF conclusions 20
6 Summary 21
7 Acknowledgement 21
8 References 22

1 Introduction: CERN North Area

1.1 CERN Accelerator Complex

CERN operates a vast variety of beam lines and accelerators, including a number of synchrotrons, transfer lines and beams for experimental facilities (see Figure 1). The latter include the beam lines for fixed target experiments, test beams and irradiation facilities at the CERN North Area (indicated by the red ellipse in Figure 1), East Area, AD/ELENA, HiRadMat and others.

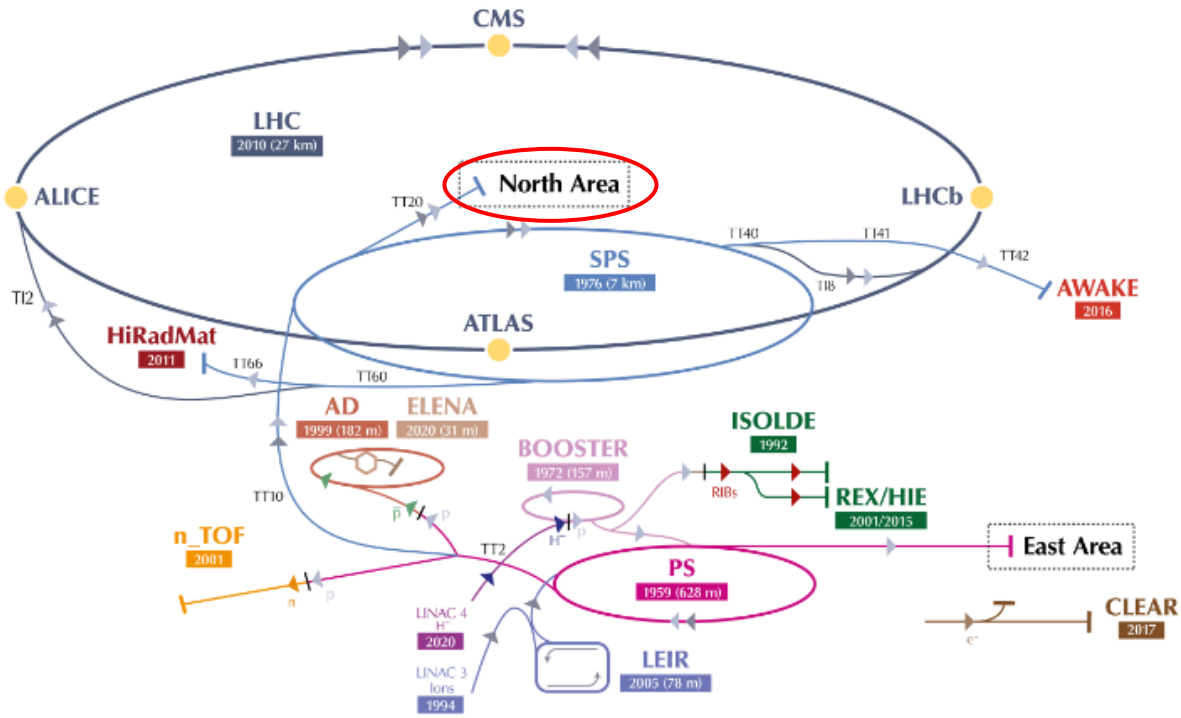

Figure 1: CERN accelerating complex with the location of the North Area indicated by the red ellipse.

1.2 SPS Extraction into the North Area

The CERN North Area receives its beam from the Super Proton Synchrotron (SPS), the second-largest synchrotron at CERN. The primary proton beam is extracted at 400 GeV/c from the SPS in so-called ‘spills’. This is indicated in the extraction supercycle displayed in Figure 2. In the diagram, the yellow curve indicates the beam intensity in the accelerator, and the white curve shows the current in the main SPS bending magnets that is proportional to the beam momentum, both as a function of time. The period corresponding to the extraction is the one where the beam intensity in the SPS is linearly reduced during the 4.8 s long spill (so-called slow extraction), while the magnetic field remains constant.

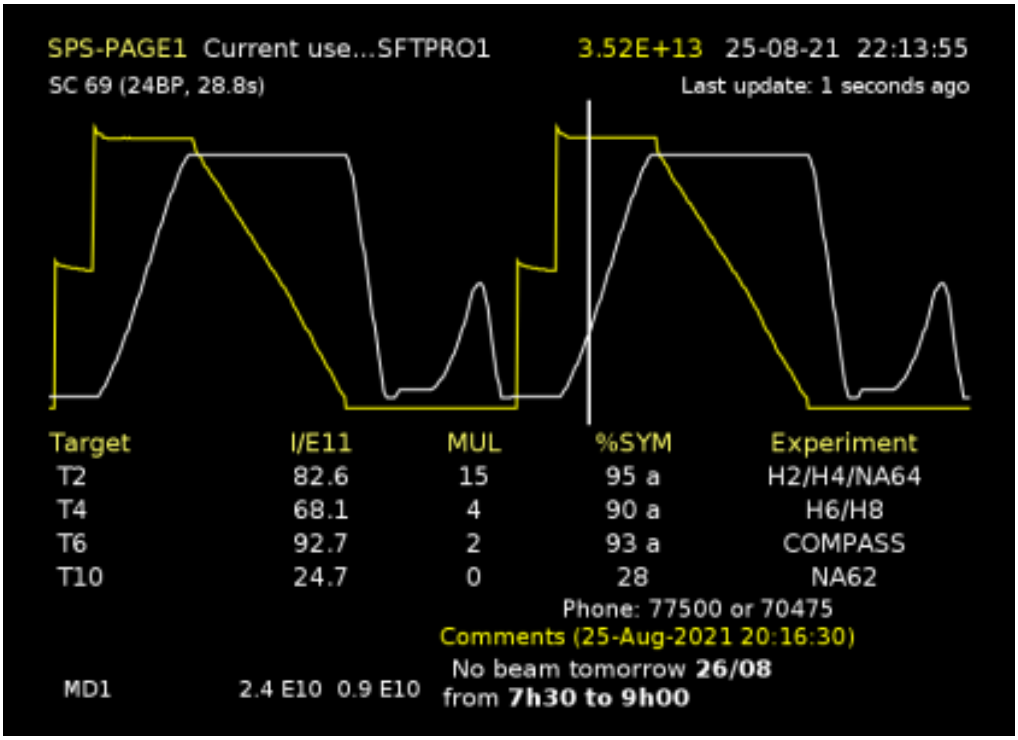

Figure 2: Screenshot of VISTAR SPS Page 1 display, indicating the extractions into the North Area (linear downwards slope sections of the yellow curve) within the SPS supercycle.

The extraction takes place once or twice per supercycle (the latter case is displayed in Figure 2), which has an overall duration between 25 and 60 seconds, depending on the scientific programme of the SPS. Prior to extraction the beam is de-bunched, so that the longitudinal distribution of the extracted particles is, in a first approximation, uniform over the period of 4.8 s.

After the extraction, the beam is split and directed towards the three North Area primary targets (T2, T4 and T6, see Figure 3). The North Area beam lines have an overall total length of about 7 km [1]. The T6 target defines the starting point of the M2 beam line, which is with 1138 m the longest fixed-target beam line in the North Area and in the world. It transports the beam to the hall EHN2, where the AMBER [2] target and detector will be located (at the bottom right in Figure 3).

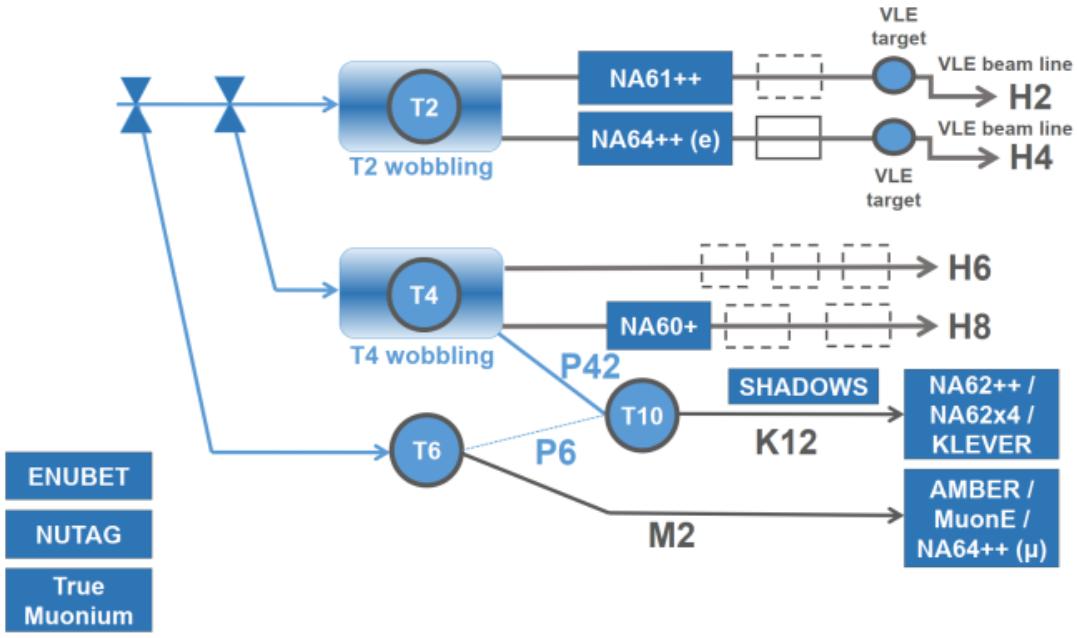

Figure 3: Schematic diagram of the North Area beam lines (apart from TT20 tunnel) and the experiments proposed in the framework of the Physics Beyond Colliders programme.

1.3 Kaon and Antiproton Rates in the M2 Beam Line

The secondary beam in the M2 line is produced at the T6 target and transported to hall EHN2. The particle production rate depends on a number of parameters and can be described by the so-called Atherton formula [3], which constitutes a parametrisation of measured particle production data from the NA20 experiment. For the calculation of the particle rates in the present sub-section (but not in the following chapters, which are describing the RF-separated beam) the following assumptions were made:

- No particle enrichment technique is used (e.g. RF separation)
- The momentum spread has an RMS value of $\Delta p/p = 1\%$
- The (full) angular acceptance of the beam line is 17.6 mSr
- The primary particle intensity on T6 corresponds to the value currently used for the COMPASS experiment, i.e. 1.5×10^{13} protons per spill
- A Beryllium target of 500 mm length is used
- The distance from T6 to the AMBER target is the full length of M2 beam line, i.e. 1138 m
- The electrons in the secondary beam are not taken into account

Based on these assumptions and taking into consideration the kaon decay rate, the absolute rates of kaons and antiprotons per spill upon arrival in the EHN2 hall are shown in the top panel of Figure 4 as a function of momentum. The curves show that the maximum rate for both types of particles is above 10^8 particles per spill, with the two maxima being at different momenta. However, without a purification or filtering technique applied, the fraction of those particles in the total intensity of the beam is in the order of a few percent, only (see Figure 4, bottom panel).

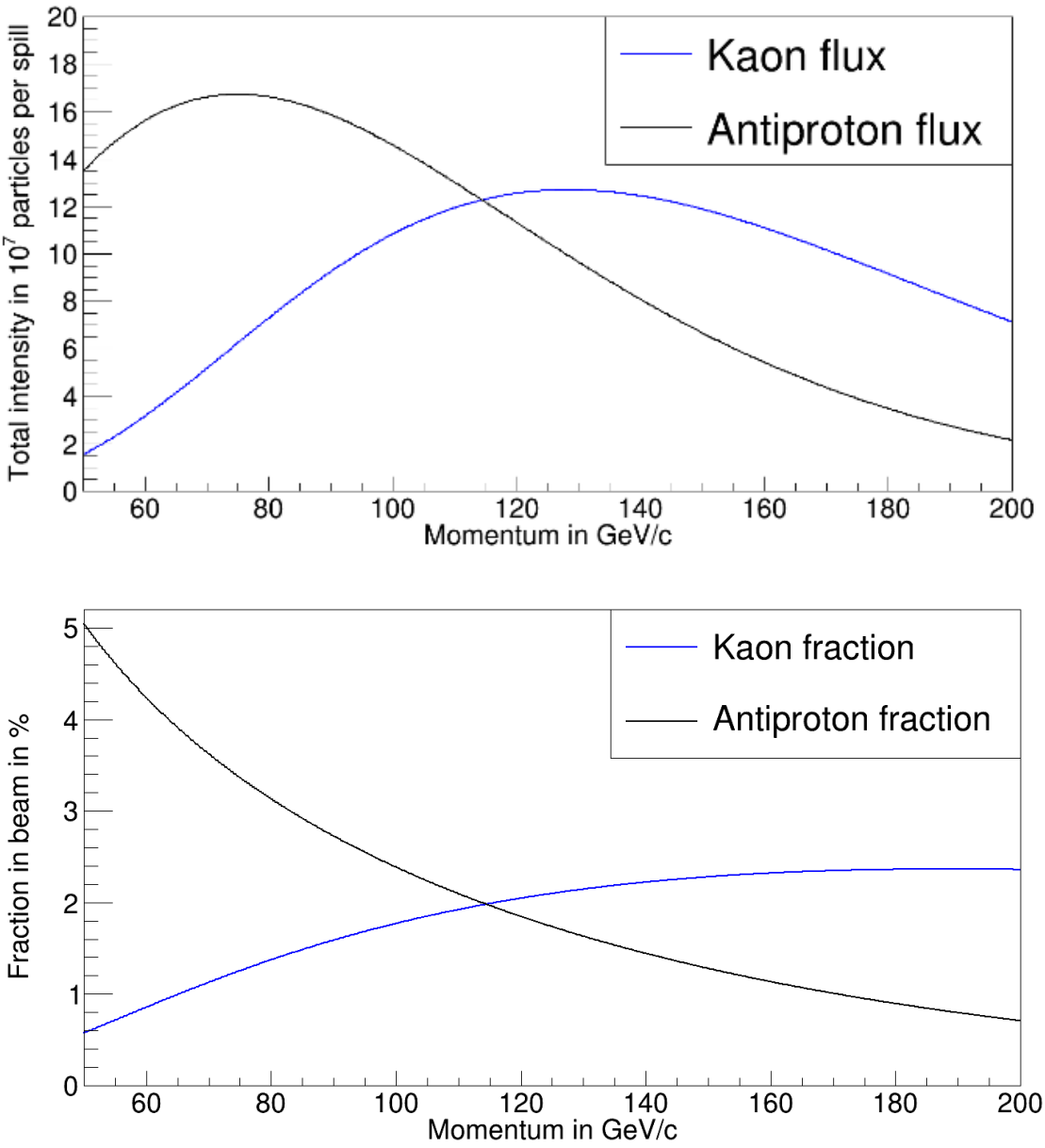

Figure 4: Top: maximal absolute intensity of kaon and antiprotons that could be delivered per spill at the AMBER location by the M2 beam line (ignoring the constraints imposed by radiation protection). Bottom: share of kaons and antiprotons in the overall beam intensity.

It is important to note that there is a Radiation Protection (RP) limitation on the overall number of hadrons per spill, which can be delivered to EHN2. This limitation, given the current layout and shielding, is at approximately $4 \cdot 10^8$ particles per spill for a configuration with a hermetic absorber following the AMBER target. A new shielding configuration is being studied, which might permit to increase this value, but the increase is expected to be moderate. For a more open configuration, in which the non-interacting part of the beam continues propagation until the end of the experimental hall, the limit is at least a factor of 5 lower, depending on the detailed layout of the experiment. Hence, assuming the present overall limit on the number of hadrons and the share of the particles of interest to be below 2.5 % for the 190 GeV hadron beam, at most 10^7 particles of the relevant type (kaons or antiprotons)

per spill can be delivered to the hall. Additionally, the maximal rate of data acquisition and triggering systems of the AMBER experiment (and of the Cherenkov counters CEDAR detector preceding it, which serves particle identification [1]) are limited, resulting in purity rate requirements much above ~2.5%. Hence a purification needs to be considered, increasing the fraction of the relevant particles in the beam and hence permitting a sufficient intensity of the relevant particle type within the RP limitations. A number of different techniques has been examined for this purpose, such as filters of material providing differential absorption, electrostatic separation and RF separation, with the examination revealing that only the latter is capable of performing adequately at the aforementioned beam energy and intensity scales.

2 Beam Requirements for Phase-2 of the AMBER Experiment

The Letter of Intent for "A New QCD facility at the M2 beam line of the *CERN* SPS (AMBER)" [4] covers all ideas for future experiments as of January 2019. A detailed proposal [2] describing the measurements foreseen in AMBER Phase-1 was submitted to the CERN SPSC later in 2019 and accepted by the CERN Research Board in 2020. A 3D sketch of the proposed AMBER layout is illustrated in Figure 5. For different experiments, different (partly disjunct) sets of detectors will be used in the front region. Data taking is scheduled to commence in 2023. In the first of the three Phase-1 experiments, the antiproton production cross sections in $p+H$ and $p+He$ scattering, which are required for a better interpretation of cosmic-ray data, will be measured at different momenta. The goal of the second experiment is the determination of the charge radius of the proton, using muon-proton scattering at 100 GeV beam energy. The third AMBER Phase-1 experiment is the measurement of the pion-induced Drell-Yan reaction, and in parallel J/ψ-production, to determine the parton distribution functions (PDFs) of the pion, i.e. its valence, sea and gluon distributions, with the goal to resolve the internal structure of the pion as Nambu-Goldstone boson of Quantum Chromodynamics (QCD) [5].

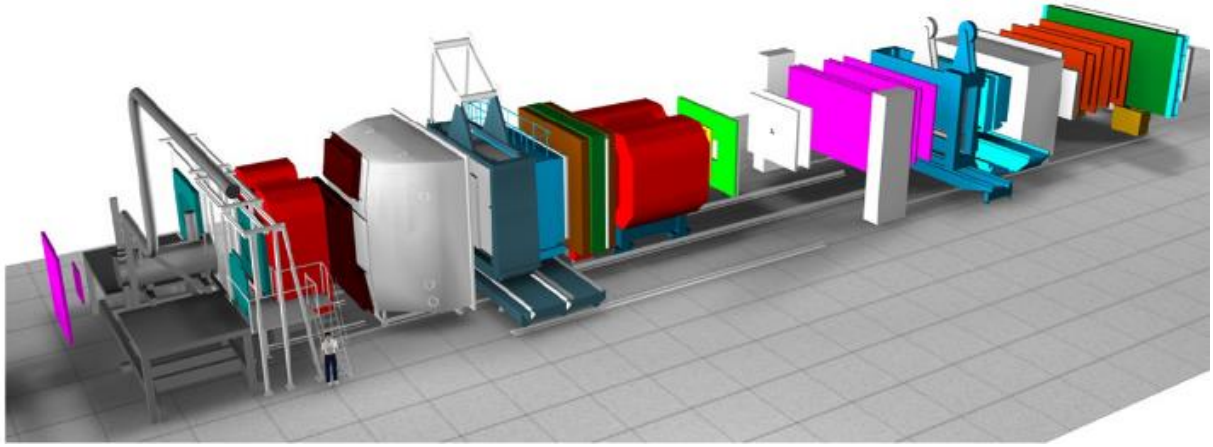

Figure 5: 3D layout of the proposed AMBER setup in EHN2 hall [2].

The physics horizon of the envisaged AMBER Phase-2 measurements has been discussed in a series of, by now, six theory workshops starting in late 2019 [6]. According to the presented state-of-the-art in QCD, the study of the Emergence of Hadron Mass (EHM) [7] [8] was chosen as appropriate Flagship Physics Goal for the AMBER Phase-2 proposal. A detailed discussion of the underlying Science Questions will be given in the proposal document that is under preparation.

Below follow short descriptions of all measurements presently envisaged for AMBER Phase-2. More detailed descriptions will be given in the proposal document. The overwhelming majority of these future

experiments require kaon beams of high intensity and (at the same time) high purity, which presumably cannot be delivered by the existing M2 beam line. Consequently, preparatory work on the beam requirements for the AMBER Phase-2 proposal was started in 2021 by initiating first studies on the possibility to use the RF-separated beam technique in the M2 beam line [9]. A detailed description of the status of these investigations is the purpose of this work and will be given starting with the next section.

The following planned measurements, summarised in Table 1, were already discussed to some detail in the Phase-2 part of the AMBER Letter of Intent. For the numbers on beam intensity it is important to distinguish between the beam intensity per spill, per second, and averaged beam intensity over a prolonged period of time. Since the spill duration is 4.8 s, the requirement on the beam intensity per spill is roughly 5 times higher than the particle rate per second during the spills. However, since the duty cycle of SPS is far below 100% due to extractions structure, time for machine development and SPS shutdowns, in order to estimate the beam intensity over a prolonged period of time, one needs to consider the average number of spills per hour, day etc. An approximate assumption of 2 spills per minute, 3000 spills per day of operation or $5 \cdot 10^5$ spills per calendar year can be made.

i) Measurements of the *kaon-induced Drell-Yan (DY) reaction* will allow us to determine the structure of the kaon by measuring its valence, sea and gluon distributions. As these distributions are almost completely unknown, every substantial new data is highly welcome. It will represent the counterpart to that of the pion-induced DY measurement that was already approved for AMBER Phase-1. Analysing both data sets together will allow for in-depth comparisons with calculational and computational QCD, e. g. on the anticipated Nambu-Goldstone nature of pion and kaon, to draw conclusions on the Emergence of Hadron mass.

ii) A first *measurement of the kaon polarisability* via the reaction $K^- Z \rightarrow K^- \gamma Z$ would be similar to the measurement of the pion polarisability performed by COMPASS [10]. It is expected to become feasible only in Phase-2 of AMBER, as the kaon component in the conventional hadron beam in Phase-1 is too small at te required high beam energies to collect the envisaged amount of data on a reasonable timescale. Also, it is difficult to identify kaons in this beam with sufficient purity. An RF-separated hadron beam, in which kaons are enriched, appears to provide a unique opportunity to perform such a measurement. Sufficient statistical accuracy can be reached in one year of data taking when using a beam of 100 GeV energy with about 10^6 kaons per spill, using a spectrometer configuration similar to one used by COMPASS.

iii) The *spectroscopy of the strange-meson sector* is widely uncharted territory. The Particle Data Group lists 25 strange mesons that have been measured in the mass range from 0.55 to 3.1 GeV/c^2 [11]. Only 12 of them are included in the summary tables, the remaining 13 states still need further clarification. The final goal is to identify all strange and light non-strange mesons in the quark-model multiplets, which would allow us to single out super-numerous states and identify multiplets beyond the quark model, including e. g. gluonic excitations. Using a beam with a kaon component of $2 \cdot 10^6$ particles per spill at the target position of the experiment would result in about one order of magnitude more events than recorded earlier using a conventional beam. This would allow for detailed Partial-Wave Analyses with accuracies as those successfully demonstrated by COMPASS for the $\pi^-\pi^+\pi^-$ final state [12]. Beam energies of at least 50 GeV are required for sufficient separation between beam and target excitations, which is mandatory for a clean identification of exclusive events.

iv) *Kaon-induced prompt-photon production* is a promising way to access the quark and gluon structure of the kaon via quark-antiquark annihilation and Gluon-Compton Scattering. In order to perform such measurements, the AMBER setup has to be equipped with a system of three electromagnetic calorimeters, similar to the COMPASS setup for Deeply Virtual Compton

Scattering (see ref. [13]). The proposed measurements require both positive and negative hadron beams with energies of at least 80 GeV; at this value with an intensity of the kaon component of at least $3 \cdot 10^6$ particles per spill. A comparable admixture of pions in the beam is welcome, as the pion-induced prompt-photon production data can be used as a reference.

As measurements of the Drell-Yan reaction require a beam-dump setup in the AMBER spectrometer, the best compromise has still to be found between the opposing requirements of highest possible beam intensity on the one hand, and radiation limits in both spectrometer and experimental hall on the other. Future studies will have to show whether the highest possible "combined" kaon intensity and purity in the M2 beam line can be reached with an improved conventional (i. e. unseparated) hadron beam, or if instead the below described RF-separated beam optimised for highest possible kaon intensity and purity will have to be preferred.

For all other presently envisaged Phase-2 measurements with a kaon beam, an open set-up in the AMBER spectrometer will have to be used. Highest possible kaon-beam purities at moderate intensities are required, which appear to be delivered best by an RF-separated beam. The beam requirements for those AMBER Phase-2 measurements that were already discussed in the Letter of Intent are summarised in

Table 2. The beam purities given in this table include the result of kaon and pion identification as provided by Cherenkov counters (CEDARs), with numbers that are expected to be similar as it was the case for earlier COMPASS measurements (see ref. [14]).

For completeness it should be mentioned that more interesting ideas were brought forward for possible AMBER Phase-2 experiments using an RF-separated beam in the M2 beam line:

i) Measure the charge radius of the kaon through elastic kaon scattering, $K^- \, e^-_{target} \rightarrow K^- \, e^-$, at low momentum transfer and, e. g., 80 GeV beam energy;
ii) Measure the $F_{K\pi\pi}$ form factor via $K\pi\pi$ production using a high-Z target.

For both ideas, feasibility studies are planned in the context of preparing the AMBER Phase-2 proposal.

Table 1: Main characteristics for the Phase-2 measurements envisaged in the AMBER Letter of Intent.

	Beam-dump setup		**Open setup**		
Name	**Drell-Yan**	**Charmonia**	**Primakoff**	**Spectroscopy**	**Prompt photons**
Underlying physics	partonic structure of Kaon	partonic structure of Kaon	ɣ-K interaction at low-t	hadron spectroscopy	partonic structure of Kaon
Process	hard	hard	Electromagnetic	diffraction	hard
Signal	$\mu^+\mu^-$ pairs	$\mu^+\mu^-$ pairs	hard ɣ	charged hadrons and photons	high-p_T ɣ
Type of measurement	inclusive	inclusive	exclusive	exclusive	inclusive

Table 2: Beam requirements for the Phase-2 measurements envisaged in the AMBER Letter of Intent

	Spectroscopy	Primakoff	Prompt photons
E=80 GeV	Perfect	Perfect	minimal possible
E=100 GeV	Perfect	Perfect	tolerant
E=120 GeV	Perfect	Perfect	perfect
Intensity (K) during the spill, 10^5 s^{-1}	4	2	8(80), 5(100), 4(120)
Beam sign	neg.	neg.	pos. + neg.
Beam purity, K/π after CEDARs	$>10^2$	$>10^3$	$>10^2$

3 RF Separated Beam for M2

The RF-separation technique achieves a discrimination of particle species based on the principle that different particles have different masses and hence at the same momentum have different velocities [15] [16]. An almost monochromatic beam with a comparably narrow momentum spread of ±1% is generated by performing momentum selection in the upstream part of the beam line (see Figure 6). Downstream of it, for the implementation of RF separation, two groups of RF cavities (with several modules each, see section 'RF Cavities & RF Power') providing a transverse kick are installed along the beam line, with the first group (RF1) reasonably close to the target and the second group (RF2) as far as possible away from the first one, in order to achieve for the different particle velocities the maximal longitudinal separation between different particle types after they traversed the distance between RF1 and RF2. Both RF1 and RF2 run at the same RF frequencies.

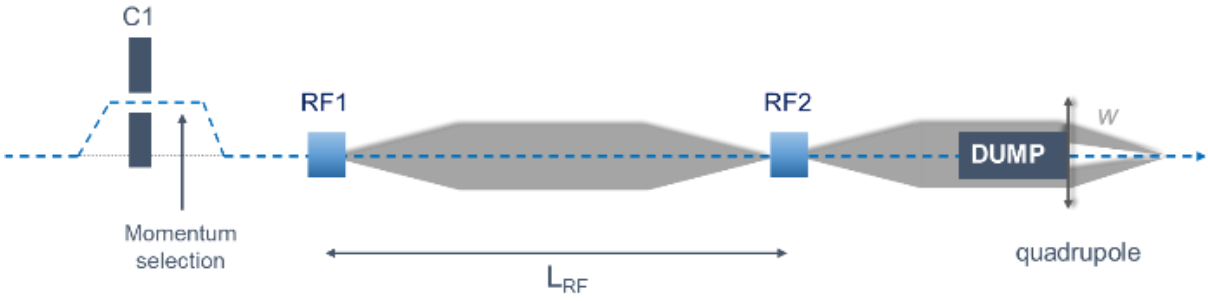

Figure 6: Illustration of RF separated beam principle.

Since the primary beam extracted from the SPS and steered onto T6 is de-bunched, the secondary beam generated at the target also has an approximately constant particle flux during the 4.8 s long spill. The particles reaching RF1 receive a time-dependent transverse kick by the RF cavities. It is important to note that the kick in RF1 depends only on the position of the particles along the RF phase, but not on the particle type. Then the particles propagate in the beam line towards RF2, with the velocity dependent on the particle type. There, the RF1 kick is either compensated or amplified by RF2, depending on the phase difference between RF1 and RF2. In the case of perfect kick compensation, the particles receive no overall kick from RF1 and RF2 and remain close to the beam axis. In the case of the kick not being compensated, the overall kick is non-zero (and ideally maximized), so that the particles are deflected by the sum of the phase-dependent kicks in RF1 and RF2. Hence, by modifying the frequency and relative

phases of the RF cavities, the particles with a specific propagation velocity can be either chosen to remain along axis and, in the case of the specific proposed design, be absorbed by the beam dump in the beam line center, or be off-axis to circumvent the dump and be later recombined with help of the quadrupoles into a focused beam (see Figure 6). With such an arrangement, in case of failure of the RF deflection system the full intensity of the beam is dumped in the beam dump and not transported towards the EHN2 hall, which otherwise would present a radiation danger to the personnel and could potentially damage the AMBER detector.

3.1 RF frequency and phase

The distance L between RF1 and RF2 ($L \approx 830\text{m}$) has been maximized in the proposed design, with the first group of the cavities being located after the first group of collimators and magnets downstream of T6, and the second group with sufficient distance upstream of the AMBER target to minimize the background of particles generated (or scattered, in case of muons) at the dump to the detector. The phase difference between RF1 and RF2 for two particles with masses m_w (w for wanted) and m_u (u for unwanted) can be calculated as

$$\Delta\varphi = 2\pi f \Delta t = \frac{2\pi f L}{c} \cdot \frac{E_\text{w} - E_\text{u}}{pc} \approx \frac{\pi f L}{c} \cdot \frac{(m_\text{w}^2 - m_\text{u}^2)c^2}{p^2} \quad (1)$$

with f being the frequency of the cavities, Δt being the difference in propagation time between RF1 and RF2, E_w and E_u being the respective particle energy and p being the momentum of the particles. Equation (1) can be reformulated to calculate the frequency required to optimally separate the two species by a given value $\Delta\varphi$:

$$f = \frac{\Delta\varphi c}{2\pi L} \cdot \frac{pc}{E_\text{w} - E_\text{u}} \approx \frac{\Delta\varphi c}{\pi L} \cdot \frac{p^2}{(m_\text{w}^2 - m_\text{u}^2)c^2} \quad (2)$$

The resulting frequency can be shown for pairs of particles with respective masses m_w and m_u. For the case of AMBER, the particles of interest are positively and negatively charged kaons as well as antiprotons, while pions and protons are the particles one intends to filter out. This should be done with help of the same hardware, in particular with regard to the frequency of RF cavities. The respective phase differences as a function of beam momentum and RF frequency are shown in Figure 7.

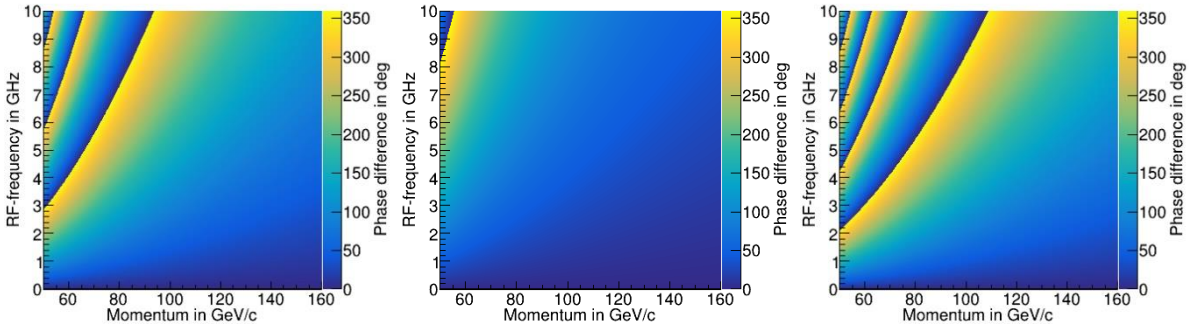

Figure 7: Kaon-antiproton (left), pion-kaon (center) and pion-antiproton (right) phase differences as a function of particle momenta and RF-frequency.

Assuming that each group of cavities, RF1 and RF2, individually provides a kick resulting in a deflection angle θ, the total angle of RF kick θ_{tot}, by which the particle is deflected cumulatively in both RF1 and RF2, can be calculated as

$$\theta_{\mathrm{tot}} = \theta\left(\sin\big(\varphi(t)\big) + \sin(\varphi(t)+\alpha)\right) = \; 2\theta\sin\left(\varphi(t)+\frac{\alpha}{2}\right)\cos\left(\frac{\alpha}{2}\right) \qquad (3)$$

with $\varphi(t)$ being the phase of the particle in the RF wave of RF1 and α being the phase difference between RF1 and RF2. The maximum of $\frac{\theta_{\mathrm{tot}}}{\theta} = 2$ is achieved if $\alpha = \pi$. However, since the particles are uniformly distributed along the phase of the RF cavities, the RMS deflection angle for a given particle type can be calculated as

$$\bar{\theta} = \sqrt{\frac{1}{2\pi}\int_0^{2\pi}\theta_{\mathrm{tot}}^2(\varphi)\,d\varphi} = \sqrt{2}\theta\cos\left(\frac{\alpha}{2}\right) \qquad (4)$$

For the case when positive kaons are the particle of interest, it is important to filter out the pions and protons, which respectively contribute to 50-70% and 20-30% of the overall beam intensity (dependent on the particle momentum). In order to filter them out effectively, one can adjust the frequency and particle momentum such that the phase difference between the protons and the positively charged pions (which is the same as for antiprotons and negatively charged pions) is $\Delta\varphi_{\mathrm{pion}}^{\mathrm{antiproton}} = 2\pi$. In that case, the phase difference between RF1 and RF2 for both of those particle types can be set to $\alpha = \pi$ and hence to propagate along the beam axis with $\theta_{\mathrm{tot}} = 0$, while the kaons receive a non-zero total deflection, as demonstrated in Figure 8.

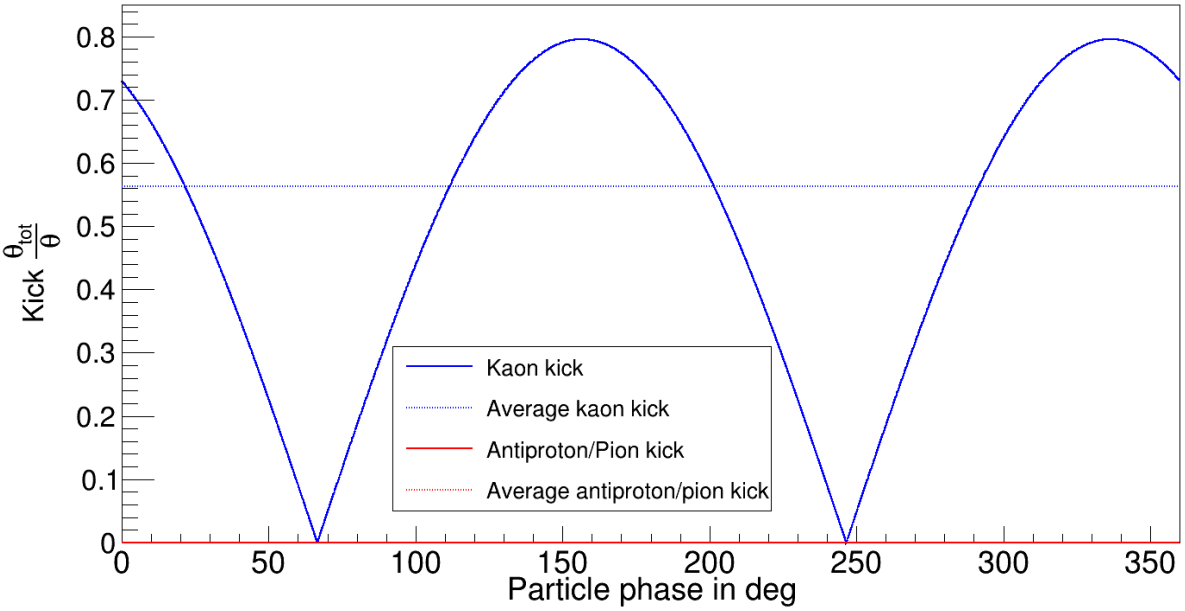

Figure 8: Illustration of deflection of pions, antiprotons and kaons for $\Delta\varphi_{\mathrm{pion}}^{\mathrm{antiproton}} = 2\pi$.

Such setting of the phase difference limits the choice of frequency and momentum of the beam to the regions depicted with yellow colour in Figure 7, bottom. Depending on the choice of RF frequency in the cavities, described in the following chapters, the optimal momentum of the beam can be selected. As an example, Figure 8 demonstrates the deflection of a beam with a momentum of 75 GeV/c and an RF frequency of $f \approx 4.72$ GHz, resulting in $\Delta\varphi_{\mathrm{pion}}^{\mathrm{antiproton}} = 2\pi$.

The same scheme cannot be used to deliver a purified antiproton beam, since for $\Delta\varphi_{\text{pion}}^{\text{kaon}} = 2\pi$ and for the momentum range of interest for AMBER (around 100 GeV/c) the frequency requirement on the RF cavity would become unrealistic, as it is demonstrated in Figure 7, middle. Furthermore, since the cost of RF cavities is not negligible, it is envisaged to utilize the same hardware (and hence the same RF frequency) for the purification of the kaon and antiproton beams. Hence, another operation mode needs to be used: for the frequency $f \approx 4.72$ GHz one can achieve a phase separation of $\Delta\varphi_{\text{pion}}^{\text{antiproton}} = \pi$ for the beam momentum of 106 GeV/c. In that case the pions can be set to $\alpha = \pi$, so that they are dumped, while the antiprotons are maximally deflected and circumvent the dump most efficiently (see Figure 9). The drawback of this operation mode is that the kaons are also somewhat deflected (although not by the same amount as antiprotons) and hence will not be completely filtered out. However, given their relatively small contribution to the beam intensity, still a significant antiproton beam purification can be achieved with this setting.

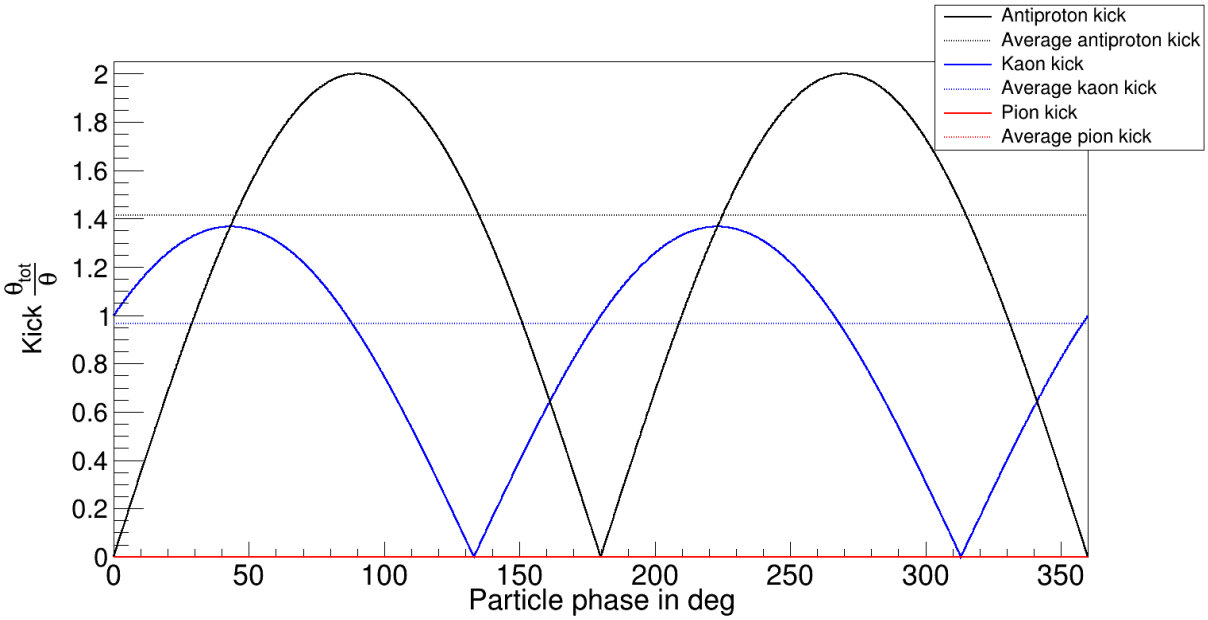

Figure 9: Illustration of deflection of pions, antiprotons and kaons for $\Delta\varphi_{\text{pion}}^{\text{antiproton}} = \pi$.

4 M2 Beam Line Considerations

4.1 Different Beam Optics Settings Scenarios

The particles of any beam do not follow precisely the nominal path, but have some non-zero offsets from the nominal trajectory in space, direction and momentum. The transverse distribution of the beam is described by the so-called emittance, which corresponds to the area that particles occupy in the transverse phase space. The emittance is conserved, unless the beam is being accelerated, decelerated, collimated or scattered (Liouville's theorem) [17]. The transport of the particles along the beam line can be described in first order by the linear algebraic approach with the so-called transfer matrices [17]. Depending on the setting of the magnets, the beam can be focused or defocused at specific locations, or be directed parallel to the nominal trajectory. With respect to the RF separated beam of M2, two major options have been considered: one with the beam being focussed at the location of the cavities and one with a parallel beam in the cavities (see Figure 10).

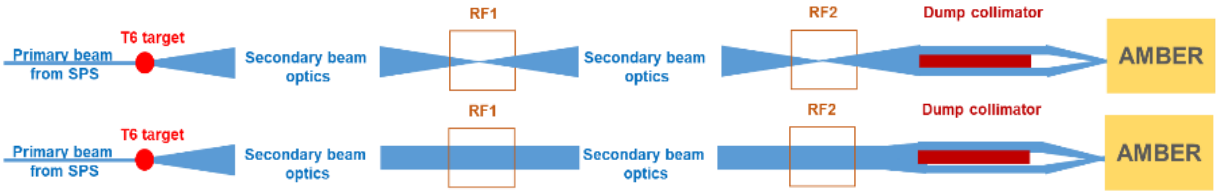

Figure 10: Illustration of RF-separated beam optics with focused (top) and parallel (bottom) beam at the location of the RF cavities.

For the focused beam the beam size in the cavities is minimized. In this case, the R_{12} and R_{34} parameters of the aforementioned transfer matrices are set to zero. This means that the initial angle of particle propagation in the transverse beam planes X and Y does not influence the offset of this particle's position in the X and Y planes at the observed location. Also, the initial divergence of the beam, which is the major contributor to the beam size along the beam line, does not influence the beam size in X and Y at this specific location. Due to the emittance conservation, this implies that the phase space ellipse occupied by the beam is small in size X, but large in divergence X', as it is demonstrated in Figure 11, top. The advantage of such setting is that the beam fits well through the aperture of the cavities, which might otherwise become a limiting factor for the transmission, as will be described below. The disadvantage of focused optics is that the relative kick provided by the cavities is small, so that the beam deflection is smaller than the divergence of the beam at this location. This means that after passing the cavities of this type, there would still be a large overlap between the deflected beam of wanted particles and the non-deflected beam of unwanted particles, resulting in a lower purity of the beam after the RF separation.

For the parallel beam the divergence of the beam in the plane of the RF kick (X in this specific design) in the cavities is minimized, implying that the R_{22} matrix parameter is zero at the location of the cavities. The beam size in the cavities is then determined by the angular acceptance of the beam line and the R_{12} parameter in the RF cavities, which, given the deflection requirements, have realistic radii up to 15 mm. Such a parallel beam is small in divergence X', but large in X (see Figure 11, bottom). The downside of this configuration is that the transmission is strongly limited by the apertures of the RF cavities. Large losses at those superconducting cavities cannot be accepted, since they would cause quenches, and hence the beam would need to be pre-collimated. On the positive side, the relative effect of the RF kick is large, since the divergence of the beam is small which allows for a better separation of the wanted particles from the unwanted ones and hence this option is capable of providing a higher purity.

Both options, the focused and the parallel beam in the RF cavities, have been considered. Also, the beam has been made as parallel as possible at the location of the CEDARs to permit maximally effective particle identification. This is due to CEDARs being able to effectively identify particles propagating with less than 60 µrad to its axis. The beam optics were developed such that the momentum resolution stays below 1%. The distance between the two groups of cavities (RF1 and RF2) was maximized ($L \approx 830$m), while maintaining the present geometry of the tunnel. The dump for the unwanted particles is located 20 m downstream of RF2 and is assumed to be 5 m long.

The purity and intensity of the beam are the crucial design goals for an RF-separated beam line. They depend on a number of beam line optics settings, such as i) the transverse beam line acceptance determined by the first six quadrupoles in the upstream part of the beam line, ii) the beam momentum spread, which impacts the differences in the time of flight of the particles, iii) the magnification factor of the parallel beam set by the R_{12} parameter at the location of the RF cavities, and iv) the RF cavity type, which determines the cavity kick, frequency, length and iris aperture.

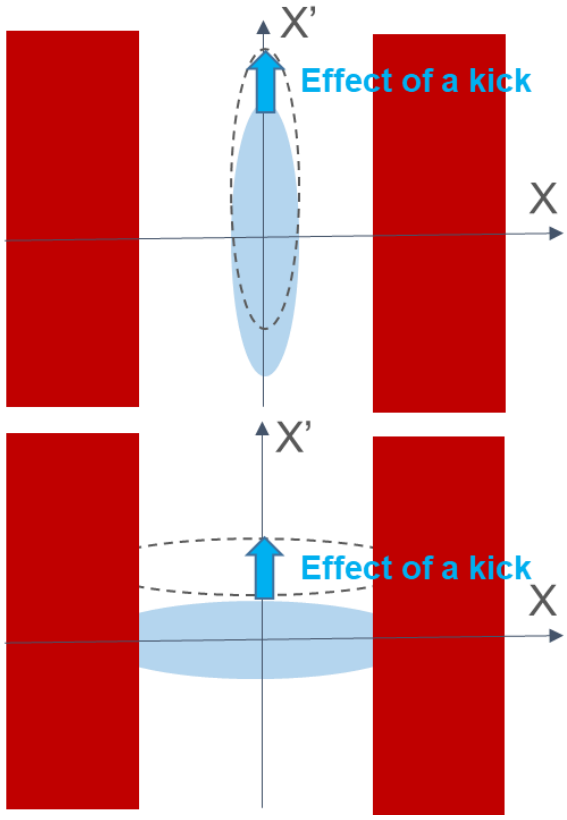

Figure 11: Illustration of the focused (top) and parallel (bottom) beam passing through the apertures of the RF cavities (in red) and receiving the RF deflection kick (indicated with the blue arrow).

4.2 Proposed Beam Line Optics

The cavities assumed for the optics design are in accordance with the parameters of the crab cavities proposed for the ILC, having an RF frequency of 3.9 GHz, a deflection gradient of 5 MV/m, an iris size of d=30 mm and a length of L=10 m for each RF1 and RF2.

Figure 12: Illustration of the beam (in blue) becoming wider during the propagation through an RF cavity (brown box) due to the RF deflection.

These parameters are crucial to determine the possible beam size at the cavity, while one must take into consideration that the cavity does not only have to be able to permit the passage of undeflected

beam, but also must contain the beam at the exit region of the cavity, which has already received the deflecting kick (see **Erreur ! Source du renvoi introuvable.**).

In the present design the beam is collimated upstream of RF1 to make sure that it fits well through the cavities, including its exit point. The width of the collimators is calculated as follows: Since the deflecting electric field is approximately homogeneous, the angle of the beam with respect to its propagation axis increases linearly in the cavities, i.e.

$$x'(z) = \frac{\frac{\mathrm{d}p}{\mathrm{d}z}}{p} \cdot z \tag{5}$$

with $\frac{\mathrm{d}p}{\mathrm{d}z}$ being the cavity gradient, p the beam momentum and z the coordinate along the beam line. The maximal size of the beam at the cavity exit can be obtained by integrating x' with respect to z, leading to

$$\sigma_{\mathrm{x}}(z) = \frac{\frac{\mathrm{d}p}{\mathrm{d}z}}{2p} \cdot z^2 + \sigma_{\mathrm{x}_0} \quad , \tag{6}$$

with x_0 being the beam size at the cavity entrance and assuming that it is perfectly parallel. To get the beam through the cavity, it should be maximally as large as the cavity iris, i.e. $x(L) = \frac{d}{2}$. This imposes the following constraint on the collimator defining x_0:

$$x_0 = \frac{1}{2}\left(d - \frac{\frac{\mathrm{d}p}{\mathrm{d}z}}{p} \cdot L^2\right) \quad , \tag{7}$$

which leads to a collimator half-opening of about 11.5 mm for the given cavity parameters and a beam momentum of 68 GeV/c.

Based on this, one can simulate the RF separation. The following diagrams are always for a negative kaon beam at a central beam momentum of 68 GeV/c, meaning that the phase difference is tuned such a way that pions and antiprotons on average do not get a kick, while the kaons are deflected, as described above. For the current set of beam optics, the resulting angular distribution behind the second cavity is shown in Figure 13.

One can clearly see that the wanted particles get an angular deflection different from 0, while the unwanted ones are efficiently filtered in terms of angle. The smearing of the distributions can be explained by the two main reasons:

1. The beam still has a non-zero divergence, which means that there are particles propagating non-parallel to the beam axis. In case that those are kaons it can happen that the angle before RF1 is compensated by the cavity kicks leading to small angles after RF2. The unwanted particles having a non-zero angle before the separation will still have this angle as the deflections in both cavities compensate one another.
2. The beam has a finite momentum resolution, because the beam line has a momentum acceptance of 1%. This leads to some kaons having momenta different from the central momentum, leading to a different phase and therefore to different deflection. The same is true for the unwanted particle species.

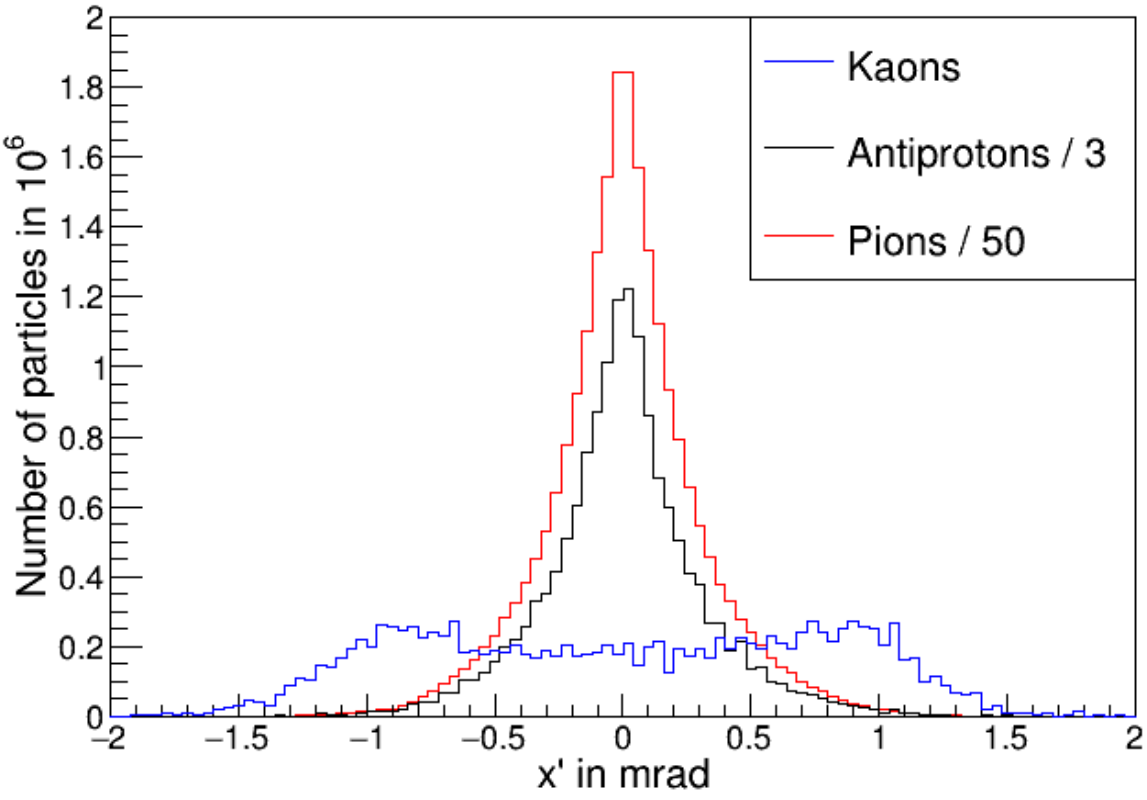

Figure 13: Angular distribution behind RF2 for a kaon beam at 68 GeV/c. For a better display of the graph a renormalization was applied: The number of simulated pions was divided by 50, while the number of antiprotons was divided by 3.

The RF-separation technique filters out different species in terms of their angles with respect to the beam axis. Obviously though, when placing a dump in the beam one does not filter out by angle, but by position. Therefore, it is necessary to translate those angular differences in particle type specific distributions into positional differences. This can be done by a simple drift, as it is demonstrated via the phase space diagrams shown in Figure 14 and Figure 15.

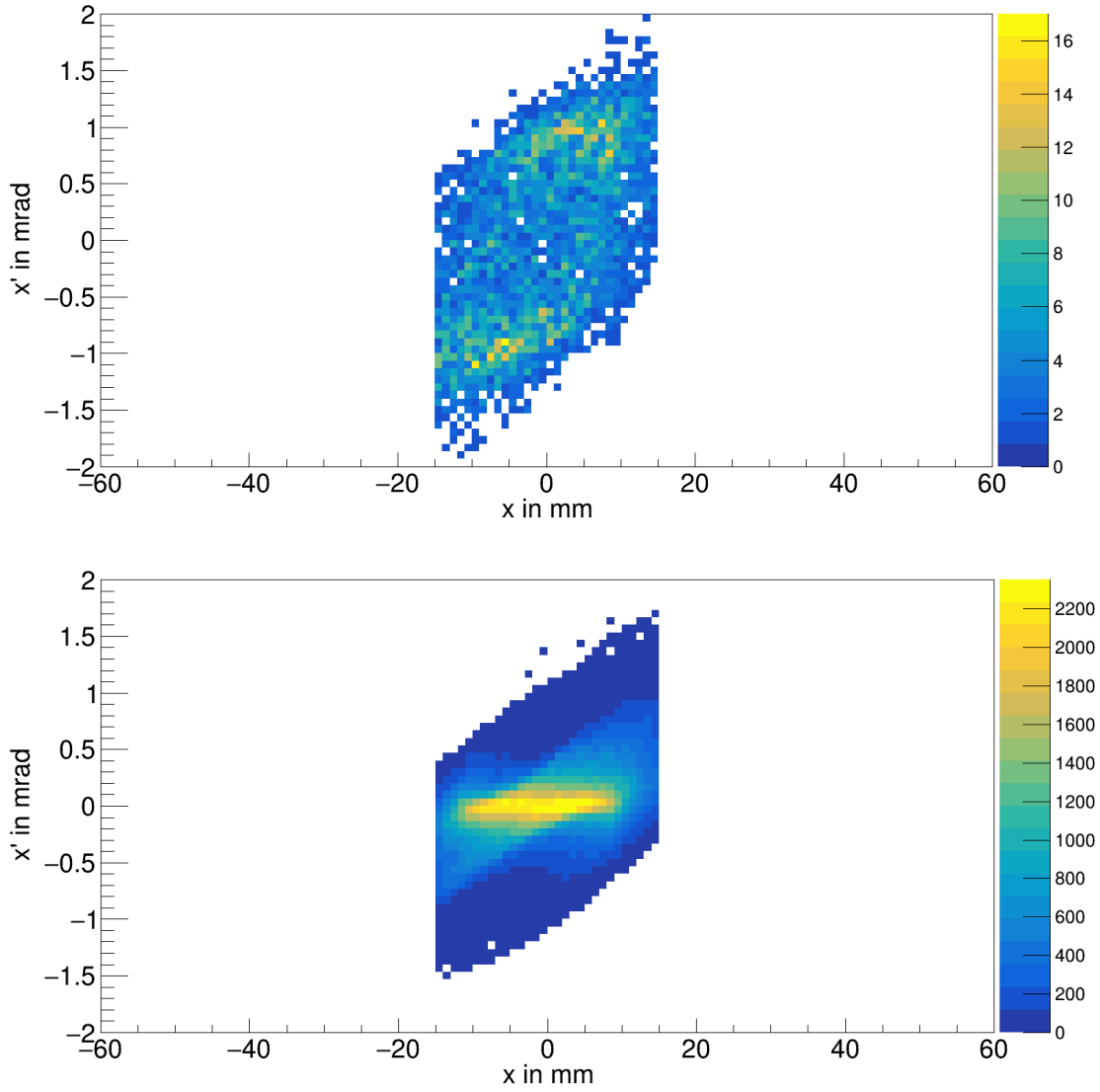

Figure 14: Phase space of kaons (top) and pions (bottom) at the exit of RF2.

At the cavity exit the spatial distributions fill out the whole cavity iris. As the kaons are the particles of interest, they have on average an angle different from zero leading to a shift of their spatial distribution, while the one for the pions will still be centred around zero after a certain drift. In the current optics design this drift is 20 m long.

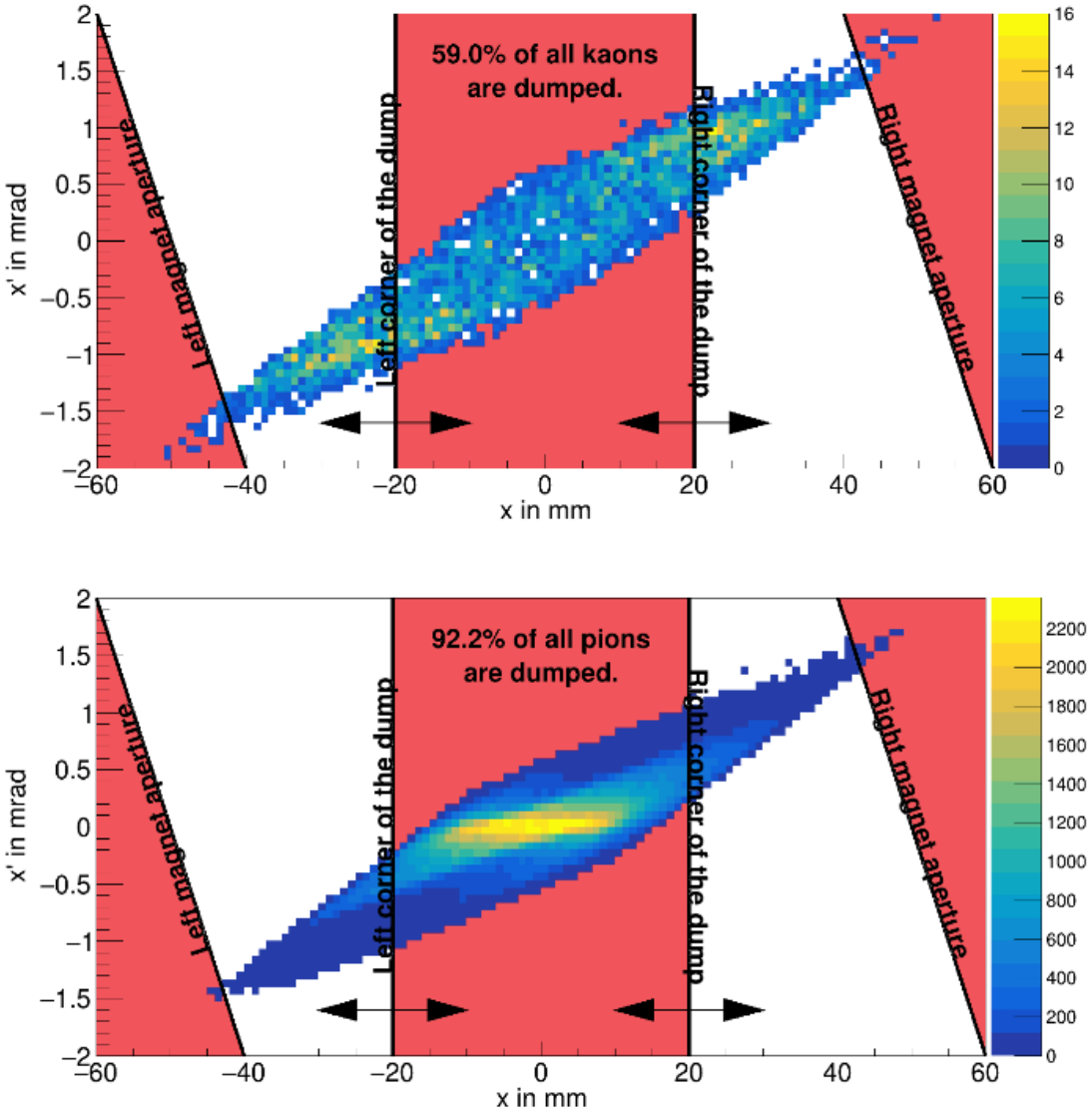

Figure 15: Phase space of kaons (top) and pions (bottom) 20 m behind RF2. The red areas indicate the regions collimated by the dump or the magnet aperture.

In Figure 15 the phase space after the 20 m long drift is shown. As expected, the pions are still located close to zero position in X-plane, while the position of kaons has changed due to the kick and subsequent drift. The two inner lines show an example of a beam dump, which is a vertical plate of material, the width of which in the X-plane (the plane of RF kick) can be modified. For a half-width of 20 mm this dump would absorb 59 % of the kaons exiting RF2, but 92 % of pions. The other two tilted lines indicate the aperture of the quadrupole behind the dump, refocussing the beam back towards the optical axis (this aperture limits the length of the drift from RF2 to the beam dump). The lines of its aperture are tilted, since the quadrupole is located downstream of the dump and hence further translation of the particle angle into the transverse position offset will take place between the dump and the quadrupole location.

In this design one can tune the kaon purity and intensity by changing the width of the beam dump downstream of RF2. Clearly, by increasing the width, the purity would increase, but the beam intensity (for both wanted and unwanted components) would decrease. Conversely, by decreasing the dump

width, one can increase the beam intensity by compromising beam purity. In Figure 16 this interplay is shown for different optics settings at the cavity locations. The starting point of the optics development is represented by the green crosses. This optics was adjusted to much smaller cavity sizes, leading to the necessity of a focus in the cavities, such that the beam could be transported. This leads to a high total transmission and therefore a high beam intensity for the reasons illustrated in Figure 11, top. But because of the focus, the relative effect of the cavity deflection is smaller, leading to a faster drop of the intensity when going to higher purities.

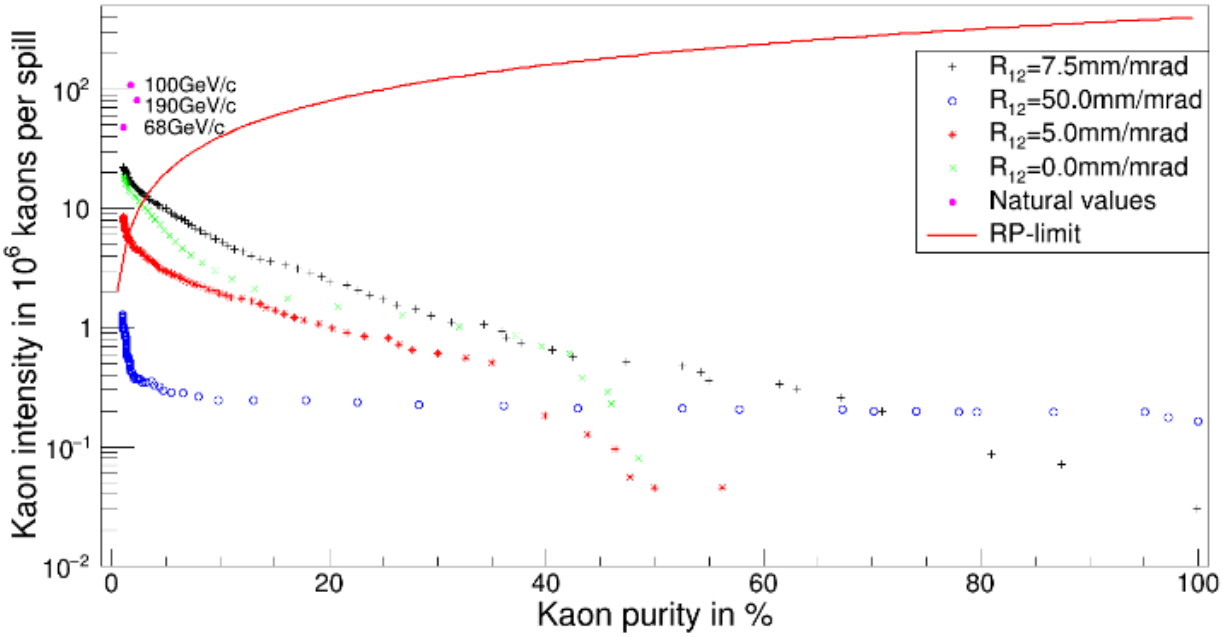

Figure 16: Kaon beam intensity depending on the kaon purity for various optics settings.

With cavities having a larger iris size it is possible to go to a parallel beam inside the cavities increasing the relative effect of the kick. When aiming at highest purities it is therefore necessary to make the beam as parallel as possible. This option is represented by the blue circles in Figure 16. There is a sharp drop of intensity at low purities, since the cavities have a finite iris and as long as the beam dump is smaller than the iris itself, one simply loses intensity without gaining much in terms of purity as all species are uniformly distributed over the cavity aperture. At higher purity levels the kaon intensity stays constant with increasing purity, as the angles of the different species are purely determined by the deflection and not by the intrinsic beam divergence. Unfortunately, the trade-off is a low overall intensity as the beam is large, leading to high losses at the collimator upstream of RF1.

The ideal option is an optics setting reaching a high intensity at a high purity. This is achieved for a beam that is as parallel as possible while still fitting through the cavity. As the beam evolution in the deflection plane is dominantly determined by the R_{12}-term in the transfer matrices, the maximal value of it can be calculated by the iris size and the acceptance of the beam line in the deflection plane. Considering only the physical iris, this would mean the beam could be fully transported through the cavities for $R_{12} = 7.5\ \mathrm{mm/mrad}$. Taking into account the reduction of the effective usable iris size due to deflection described at the beginning of the present section, this reduces to $R_{12} \geq 5\ \mathrm{mm/mrad}$. A setting like this is less performant in terms of separation, but for the experiment it is important to still have a high intensity at a reasonable purity. For that reason, the transmission along the whole M2 beam line has been optimized for the black crosses in Figure 16. This can be seen in the fact that the total intensity for a parallel beam setting is higher than for the optics aiming at a focus in the cavities.

Considering the black crosses in Figure 16, with the corresponding set of optics one is able to provide a kaon intensity of 10^6 per spill at the AMBER target of 40% purity. Allowing a lower purity of 20%, one can reach already a rate that is three times higher, i.e. $3 \cdot 10^6$ kaons per spill. In both cases, one would be far below the radio-protection limit shown (red solid curve in Figure 16) in the experimental hall, where the AMBER experiment will be located.

Considering the RP-limit of $4 \cdot 10^8$ particles per spill, everything above the solid red curve would be too high intensity, meaning that the rate still would need to be decreased.

4.3 Conclusions from Beam Line Optics Examination

With the currently achieved beam intensity and purity by RF separation, it will possible to reach the goals set for the AMBER Phase-2 measurements of the kaon charge radius, the Primakoff reaction, prompt-photon production and kaon spectroscopy. In contrast, the high beam intensities in the order of 10^8 particles per spill needed for the Drell-Yan studies cannot be provided with the RF-separation technique on the basis of the current radiation protection limitations, given the length of M2 beam line and the technical capabilities of the cavities. For this reason, the conventional M2 hadron beam is currently revised to improve the number of kaons reaching EHN2. As those are identified by Cherenkov counters before entering the hall, it is necessary to tag as many of them as possible. This, in turn, requires a more parallel beam at the CEDAR location, which is also under investigation at the moment.

5 RF Cavities & RF Power

As discussed in the sections above, the parameters of the RF-deflection system have a large impact on the performance of the RF-separated beam technique. Large deflecting voltage, large iris size, high RF frequency and low cost would be an ideal combination, but in reality these requirements are mutually in conflict and hence a compromise needs to be found. Different sets of requirements for the RF system have been considered, which led to the consistent set of requirements summarized in Table 3.

Table 3: RF requirements

Deflecting voltage per RF station	50 MV
RF Frequency range	Above 3 GHz
Spill length	4.8 s
Repetition rate	10 s – 50 s
Beam aperture	~30 mm

5.1 Cavity requirements

In RF terms, a spill length of ~5 s means that the RF structures need to sustain the heat load of continuous wave (CW) operation. This excludes the use of normal conducting cavities as the deflection voltage per meter would have to be very low in order to reduce surface heating, thereby lengthening the RF sections to impractical values. Hence superconducting (SC) cavities are considered in the following, which have the additional advantage that larger apertures can be realized.

Deflecting cavities or crab cavities are typically used in colliders to reduce the loss of luminosity caused by the finite beam crossing angle at the collision. The International Linear Collider Study (ILC) considers 9-cell 3.9 GHz dipole cavities [18] for this purpose and here we use this design to estimate the number of needed cavities and the RF power (see Table 4). Using a realistic deflection voltage of ~2 MV/cavity a total of 24 cavities provides 50 MV per RF station. As typical RF cryomodules contain around 8 cavities, M2 beam line would have three modules of ~6 m at each of the two RF stations, RF1 and RF2.

5.2 RF power

The RF power needed at the cavity input (P_{in}) is determined by the sum of the dissipated RF power on the cavity surfaces (P_{diss}), the beam loading (power given to the beam, P_b), and the power (P_{stab}) needed to stabilize the cavity frequency against small oscillations (Δf) caused by microphonics. As the dissipated power (parameters see Table 4)

$$P_{diss} = \frac{V^2}{\left(\frac{R}{Q}\right)Q_0} \approx 6\ \mathrm{W} \tag{8}$$

and the power given to the beam [$O(\mu W)$] are negligible, the cavity RF input power is only determined by the constraints to keep the cavities on tune. In the above equation V stands for the deflecting voltage, (R/Q) is the figure of merit for the deflecting cavity mode, which depends only on the cavity geometry, and Q_0 is the quality factor of this mode. The RF input power to keep the cavities on tune for maximum frequency deviations Δf is defined by [19]

$$P_{in} = \frac{V^2}{4(R/Q)Q_{ex}}\left(1 + \left(2Q_{ex}\frac{\Delta f}{f}\right)^2\right) \tag{9}$$

where all quantities are related to the dipole deflecting mode. Assuming that the quality factor Q_{ex} related to the generator impedance and the quality factor Q_l of the loaded cavity are equal, we can use this equation to estimate an optimum Q_l to minimize the power consumption for a realistic maximum detuning (e.g. $\Delta f \leq 1$ kHz). At a $Q_l = 2 \times 10^6$ we find that ~5 kW per cavity are needed to keep the cavities on tune. It should be noted that a better frequency stabilization, e.g. to a level of $\Delta f \leq 100$ Hz, may be reached with a Ferroelectric Fast Reactive Tuner (FeFRT) [20], which would then reduce the power needs per cavity to less than 1 kW (at $Q_l = 1 \times 10^7$).

In order to reduce the cost of the RF power system it is recommended to choose RF sources that are readily available from the manufacturers. In this frequency and power range the only available sources today are klystrons. At 3.9 GHz specifically, the authors found one manufacturer that can supply 3 kW tubes, which would be suitable for a frequency bandwidth slightly below 1 kHz.

5.3 RF conclusions

A draft layout for the RF system was made based on existing ILC cavity designs. At each of the 2 RF stations 3 cryomodules with 24 9-cell cavities will be needed to achieve 50 MV of deflecting voltage. This corresponds to ~20 m of beamline per station dedicated to RF cavities. The resulting set of parameters is summarized in Table 4. While all these values are achievable, all parameters (RF frequency, cryogenic temperature, cavity bandwidth, power needs, aperture, etc.) should be optimized to increase the particle yield and to reduce RF power consumption. One potential optimization might include the circular polarization of the RF kick, hence providing deflection (and resulting particle purification) in both X and Y dimensions simultaneously. This option would require a recalculation of the beam optics and a redesign of the beam dump.

Table 4: SC cavity parameters for AMBER, extrapolated from ILC Crab Cavities.

RF frequency (f)	3.9 GHz
Cells per cavity	9
Active length per cavity	0.34 m
Aperture radius	15 mm
Deflection	6.1 MV/m
Deflection per cavity (V)	2.08 MV
Cavities per RF station	24
Cavities per cryomodule	8
Cryomodules per RF station	3
Cryomodule length	~6 m
R/Q (transverse)	235 Ω
Q_0 @70 nΩ, 1.8K	3.2×10^9
Q_l (loaded Q for 1 kHz phase stabilization)	2×10^6
P_{in} (power needed at cavity input)	≤ 5 kW
Expected number of particles per spill passing through the cavities	$< 1 \times 10^{10}$

6 Summary

Phase-2 of the AMBER experiment, which is being proposed for operation at the M2 beam line of the CERN North Area complex, requires a higher intensity and purity of kaon (priority 1) and antiproton (priority 2) beams than currently delivered by the beam line. The share of kaons and antiprotons in the beam is limited by their production rate at the primary target and the kaon decay along the more than 1.1 km long beam line. Furthermore, the overall intensity of the beam is limited by radiation protection considerations in the EHN2 hall that is proposed to host the experiment.

The RF-separated beam technique is an option to increase the share of kaons and/or antiprotons in the M2 beam. Different beam optics settings have been examined and extensive tracking simulations have been performed, optimizing the beam intensity and purity of the potential RF-separated beam. This was done in close collaboration with the RF group at CERN and hence based on realistic expected parameters of the RF cavities.

No show stoppers were identified for a possible RF-separated M2 beam to deliver the required intensities and purities for the envisaged AMBER Phase-2 measurements of kaon spectroscopy, prompt-photon production, Primakoff reactions and kaon charge radius. Hence it is foreseen to continue the feasibility and conceptual design study. Concerning the very high beam intensities required for the kaon-induced Drell-Yan data taking programme of AMBER Phase-2, however, it has been found that the RF-separated beam technique does presently not meet the expectations. Hence alternative scenarios for the improvement of particle identification by the CEDAR Cherenkov detectors need to be examined, which include the installation of additional vacuum, modification of beam optics and modifications of the CEDAR design.

7 Acknowledgement

The authors would like to warmly thank Alexej Grudiev, Walter Wuensch, Graeme Campbell Burt, Leo Bellantoni, Augusto Ceccucci and Marcia Quaresma for their contributions to the discussions on

beam requirements and RF-cavity capabilities. The continuous support by Craig Roberts in developing the AMBER physics case is highly acknowledged.

8 References

[1] D. Banerjee, J. Bernhard, M. Brugger, N. Charitonidis, N. Doble, L. Gatignon and A. Gerbershagen, "The North Experimental Area at the Cern Super Proton Synchrotron," CERN Document Server, CERN-ACC-NOTE-2021-0015, 2021.

[2] B. Adams et.al., "COMPASS++/AMBER: Proposal for Measurements at the M2 beam," CERN-SPSC-2019-022, SPSC-P-360, CERN, Geneva, 2019.

[3] H. W. Atherton, C. Bovet, N. T. Doble, L. Piemontese, A. Placci, M. Placidi, D. E. Plane, M. Reinharz, E. Rossa and G. V. Holtey, "Precise measurements of particle production by 400 GeV/c protons on beryllium targets," CERN Yellow Reports: Monographs, CERN-80-07, CERN, Geneva, 1980.

[4] B. Adams et.al., "Letter of Intent: A New QCD facility at the M2 beam line of the CERN SPS (COMPASS++/AMBER)," arXiv:1808.00848, Tech. rep., CERN-SPSC-2019-003 (SPSC-I-250).

[5] T. Horn and C. Roberts, "The pion: an enigma within the Standard Model," *J. Phys.,* vol. G 43, pp. 073001/1-46, 2016.

[6] "Perceiving the Emergence of Hadron Mass through AMBER@CERN," 2021. [Online]. Available: https://indico.cern.ch/event/1063883/.

[7] C. D. Roberts, "Perspective on the origin of hadron masses," *Few Body Syst.,* vol. 58, p. 1, 2017.

[8] C. D. Roberts et.al., "Insights into the Emergence of Mass from Studies of Pion and Kaon Structure," *https://arxiv.org/abs/2102.01765; acc. for publ. in Prog. Part. Nucl. Phys.,* 2021.

[9] "RF-separated beams for Amber- Kick Off Meeting," CERN, Oct. 2021. [Online]. Available: https://indico.cern.ch/event/1069879/.

[10] C. Adolph et.al., "Measurement of the charged-pion polarisability," *Phys. Rev. Lett.,* vol. 114, p. 062002, 2015.

[11] P. A. Zyla et.al., "The Review of Particle Physics," *Prog. Theor. Exp. Phys.,* p. 083C01, 2020.

[12] M. Aghasyan et.al., "Light isovector resonances in $\pi^- p \to \pi^- \pi^- \pi^+ p$ at 190 GeV/c," *Phys. Rev.,* vol. D 98, p. 092003, 2018.

[13] R. Akhunzyanov et.al., "Transverse Extension of Partons in the Proton probed by Deeply Virtual Compton Scattering," *Phys. Lett.,* vol. B 793, p. 188, 2019.

[14] P. Abbon et. al., "The COMPASS setup for physics with hadron beams," *Nucl. Instr. Meth.,* vol. A779, p. 69, 2015.

[15] W. Schnell, "Discussion of a radio-frequency particle separator for the CERN Proton Synchrotron," CERN 61-5, CERN, Geneva, 1961.

[16] W. K. H. Panofsky, "A Mass Sensitive Deflector for High Energy Particles," HEPL-82 (Internal Memo), High Energy Physics Laboratory, Stanford University, Stanford, California, 1956.

[17] E. Wilson, An Introduction to Particle Accelerators, Oxford, UK: Oxford University Press, 2001.

[18] C. Adolphsen, "Design of the ILC Crab Cavity System," EUROTeV-Report-2007-010, 2007.

[19] J. Tuckmantel, "Cavity-Beam-Transmitter Interaction Formula Collection with Derivation," CERN-ATS-Note-2011-002 TECH, Geneva, Switzerland, 2011.

[20] N. Shipman, "Ferroelectric Fast Reactive Tuner Application for SRF Cavities," in *IPAC*, 2021.